HHS Public Access

Author manuscript

Proc SPIE Int Soc Opt Eng. Author manuscript; available in PMC 2016 October 05.

Published in final edited form as:

Proc SPIE Int Soc Opt Eng. 2015 ; 2015: . doi:10.1117/12.2082121.

Construction of Realistic Liver Phantoms from Patient Images using 3D Printer and Its Application in CT Image Quality Assessment

Shuai Leng[1], **Lifeng Yu**[1], **Thomas Vrieze**[1], **Joel Kuhlmann**[2], **Baiyu Chen**[1], and **Cynthia H. McCollough**[1]

[1]Department of Radiology, Mayo Clinic, Rochester, MN, 55905

[2]Division of Engineer, Mayo Clinic, Rochester, MN, 55905

Abstract

The purpose of this study is to use 3D printing techniques to construct a realistic liver phantom with heterogeneous background and anatomic structures from patient CT images, and to use the phantom to assess image quality with filtered backprojection and iterative reconstruction algorithms. Patient CT images were segmented into liver tissues, contrast-enhanced vessels, and liver lesions using commercial software, based on which stereolithography (STL) files were created and sent to a commercial 3D printer. A 3D liver phantom was printed after assigning different printing materials to each object to simulate appropriate attenuation of each segmented object. As high opacity materials are not available for the printer, we printed hollow vessels and filled them with iodine solutions of adjusted concentration to represent enhance levels in contrast-enhanced liver scans. The printed phantom was then placed in a 35×26 cm oblong-shaped water phantom and scanned repeatedly at 4 dose levels. Images were reconstructed using standard filtered backprojection and an iterative reconstruction algorithm with 3 different strength settings. Heterogeneous liver background were observed from the CT images and the difference in CT numbers between lesions and background were representative for low contrast lesions in liver CT studies. CT numbers in vessels filled with iodine solutions represented the enhancement of liver arteries and veins. Images were run through a Channelized Hotelling model observer with Garbor channels and ROC analysis was performed. The AUC values showed performance improvement using the iterative reconstruction algorithm and the amount of improvement increased with strength setting.

Keywords

3D Printing; phantoms; heterogeneous background; lesion detection; model observer; Channelized Hotelling Observer

1. INTRODUCTION

With concerns on increased radiation dose from medical imaging, a large collection of dose reduction methods have been investigated, such as automatic exposure control, optimized kV selection, projection or image based denoising techniques, and iterative reconstruction [1-8]. To follow the ALARA principle (As Low As Reasonable Achievable), lowest radiation dose

that can be used without sacrificing diagnostic performance should be used. To address the question, “how low can we go”, an objective assessment of image quality is needed. This is particular important for iterative reconstruction and denoising techniques that involve in non-linear processes. Conventional image quality metrics, such as modulation transfer function (MTF), noise power spectrum (NPS) and contrast to noise ratio (CNR) may not be sufficient to evaluate image quality in these scenarios. For example, recent studies reported degraded low contrast detectability using IR and decreased radiation doses, although conventional image quality is still maintained [9-11]. Task based image quality metrics based on model observers have gained popularity in CT image quality evaluation, especially for application in image quality assessment of iterative reconstruction [12-18]. Several previous studies have demonstrated a good correlation between the performance of human observer and model observer [15-17]. Most of these studies were performed using phantoms with uniform background due to their simplicity and wide availability. However, to assess image quality and radiation dose reduction in clinical CT imaging, physical phantoms having realistic background textures and lesions are highly desirable as performance may be affected by anatomic background [19]. Although anthropomorphic phantoms are commercially available, they are usually not patient specific and are difficult to customize. 3D printing techniques have been widely used in industry and recently their application in medicine has been explored [20-23]. Compared to conventional phantom manufacturing, 3D printing techniques have the advantage of flexibility which allows users to quickly manufacture patient specific phantoms. Therefore, the purpose of this study is to construct a realistic liver phantom with lesions using 3D printing technique and to use this phantom for task-based image quality assessment of filtered backprojection and iterative reconstruction algorithms.

2. METHODS AND MATERIALS

2.1. Liver phantom construction

The 3D printer (Objet 350 Connex, Stratasys, MN) used in this study is based on PolyJet 3D printing technique, which is similar to inkjet printing technique but jetting layers of curable liquid photopolymer onto a build tray to build smooth and detailed 3D models. The general procedure of 3D printing using this printer can be summarized in 4 major steps, as shown in the following flowchart (Figure 1).

1) Data acquisition: In this study, we used patient images from a contrast enhanced liver CT scan performed in the portal venous phase. The patient was scanned on a 128 slice scanner (Definition Flash, Siemens Healthcare, Forchheim, Germany) with 100 kV, 445 effective mAs and 18 mGy volume CT dose index ($CTDI_{vol}$). The images were reconstructed using a medium sharp kernel (B40) at 3 mm slice thickness.

2) Segmentation: Patient images were then loaded into a commercial software (Mimics, Materialise, Belgium) for segmentation. Multiple automatic and manual segmentation methods were used during this procedure, including thresholding, region growing, morphology operations, and multi-slice editing. For the purpose of our study, the images were segmented into liver tissues,

liver lesions, and liver vessels (Figure 2a). To reflect the heterogeneity of liver background, liver tissues were segmented into two groups based on the CT numbers (Figure 2b).

3) Processing: Segmented data were then processed to generate digital models using another commercial software (3Matic, Materialize, Belgium). Wrapping and fixing were usually conducted to remove abrupt changes at model boundary and eliminate bad triangles before outputting the stl files for each segmented object.

4) The stl files were then loaded to the 3D printer (Objet350 Connex, Stratasys, MN) to print the phantom. Available printing materials were scanned on a CT scanner to determine the CT number of each material, based on which the different type of printing materials were assigned to each object in the liver phantom.

2.2. Model observer study

The printed phantom was then placed in a 35 × 26 cm oblong-shaped water phantom which simulates the attenuation of the abdomen for a standard size adult patient. The whole phantom was scanned on a 192 slice CT scanner (Definition Force, Siemens Healthcare, Forchheim Germany). Automatic exposure control (CareDose 4D) was turned on with quality reference mAs of 80, 120, 160, and 200, which corresponded to volume CTDI ($CTDI_{vol}$) of 5.2, 7.7, 10.2, and 12.8 mGy. At each dose level, the phantom was scanned 100 times. Another phantom without the lesion (all the rest are the same) was also constructed and scanned 100 times using the same techniques as those of the phantom with lesion. Images were reconstructed at 3 mm slice thickness and 250 mm field of view, using both standard filtered backprojection with a medium sharp kernel (Br40) and an iterative reconstruction algorithm (ADMIRE, Siemens Healthcare) with 3 different strength settings (IR-3, IR-4 and IR-5). These images were analyzed using a channelized Hotelling model observer (CHO) to determine the AUC of the lesions at various imaging conditions [1-3].

The general form of the test statistics for a linear model observer is the inner product between the observer template and the image, which yields a scalar response given by $\lambda=\omega^{t}g=\sum_{n=1}^{N^2}\omega_n g_n$, where the vector g denotes an image and ω a template. The template in the CHO observer is given by $\boldsymbol{\omega}_{\mathbf{CHO}}=S_c^{-1}[\overline{g}_{sc}-\overline{g}_{bc}]$, where $S_c=\frac{1}{2}[K_{sc}+K_{bc}]$ is the intraclass channel scatter matrix and $\overline{g}_{sc}$ and $\overline{g}_{bc}$ are the channel output means of signal plus background and background: $\overline{g}_{sc}=U^T\overline{g}_s, \quad \overline{g}_{bc}=U^T\overline{g}_b$. In this study, Gabor channels were selected using 4 passbands, 5 orientations, and 2 phases (a total of 40 channels), the same as in previous publications [13, 16]. For each condition (dose and reconstruction algorithm), ROC curves were generated based upon the test variables of the 200 realizations (100 signal and 100 background). Area under the ROC curve (AUC) was calculated using a non-parametric approach and served as the figure of merit. Internal noise, proportional to the variance of test variables from the background images, was added to the model observer while calculating AUC.

3. RESULTS

The measured CT number for available printing materials ranged from 62 to 117 HU, as shown in Figure 3. These CT numbers are in appropriate range for soft tissues and the difference between the printing materials provides appropriate contrast between liver tissues and low contrast liver lesions. However, the CT numbers of these printing materials are not sufficient to represent contrast enhanced vessels inside the liver. To accommodate this, we printed hollow vessels and filled these vessels with iodine contrast. By adjusting the concentration of iodine contrast, vessels with different amount of enhancement were generated.

Figure 4a shows a photograph of the printed liver phantom. Two subtle color changes on the surface represent the two different materials used for the liver tissues. The holes in the phantom are the openings of the vessels, which can be filled with iodine solutions at different concentrations. Figure 4b shows a CT image of the physical phantom scanned in air. Variation of CT numbers in the area with liver tissues represents the background heterogeneity of liver CT images, which potentially represents patient's anatomy better than the uniform background. The low contrast lesion and high contrast vessels can all be appreciated from this image.

Figure 5 shows the CT images of the liver phantom scanned in the 35 × 26 cm oblong-shaped water phantom that represents the abdomen of a standard adult patient. The four rows show images at 4 dose levels from 5.2 mGy to 12.8 mGy. Each column shows images reconstructed with one of the four algorithms (FBP and IR at strengths of 3, 4 and 5). It can be observed from these images that noise increases with decreased radiation dose. Additionally, the lesion becomes less visible with decreased dose. For the same dose, images reconstructed with IR show lower noise compared to those reconstructed with FBP. For different IR strength settings, noise is lower for images with stronger setting (higher IR strength).

The AUCs of ROC curves after running through CHO are shown in Figure 6. AUC values increased with increased radiation dose, as expected. At each dose level, the AUC values from images reconstructed with IR had higher values than that from images reconstructed with FBP. AUC increased with IR strength settings, i.e. IR-5 has the highest AUC values.

4. CONCLUSIONS AND DISCCUSSIONS

This work provides a method to construct realistic anthropomorphic phantoms with heterogeneous background and anatomic structures (e.g. lesions and vessels) based on patient CT images and using a 3D printer. We demonstrate the application of this phantom to assess image quality and lesion detection in the context of realistic background textures using CHO. The phantoms can enable the determination of the effect of radiation dose reduction and noise reduction techniques on the detectability of subtle liver lesions in realistic texture backgrounds.

ACKNOWLEDGEMENTS

This work is partially supported by NIH grants R01 EB017095 and U01 EB017185.

REFERENCES

[1]. McCollough C, et al. Achieving Routine Sub-mSv CT Scanning: Report from the Summit on Management of Radiation Dose in CT. Radiology. 2012; 264(2):567–80. [PubMed: 22692035]

[2]. McCollough CH, Bruesewitz MR, Kofler JM Jr. CT dose reduction and dose management tools: overview of available options. Radiographics. 2006; 26(2):503–12. [PubMed: 16549613]

[3]. Yu L, et al. Automatic selection of tube potential for radiation dose reduction in CT: A general strategy. Med Phys. 2010; 37(1):234–43. [PubMed: 20175486]

[4]. Yu L, et al. Radiation dose reduction in computed tomography: techniques and future perspective (PMC3271708). Imaging in Medicine. 2009; 1(1):65–84. [PubMed: 22308169]

[5]. Kalender WA, Wolf H, Suess C. Dose reduction in CT by anatomically adapted tube current modulation. II. Phantom measurements. Med Phys. 1999; 26(11):2248–53. [PubMed: 10587205]

[6]. La Rivière PJ, Bian J, Vargas PA. Penalized-likelihood sinogram restoration for computed tomography. IEEE Trans. Med. Imaging. 2006; 25(8):1022–1036. [PubMed: 16894995]

[7]. Wang J, et al. Penalized weighted least-squares approach to sinogram noise reduction and image reconstruction for low-dose X-ray computed tomography. IEEE Trans Med Imaging. 2006; 25(10):1272–83. [PubMed: 17024831]

[8]. Thibault JB, et al. A three-dimensional statistical approach to improved image quality for multislice helical CT. Med Phys. 2007; 34(11):4526–44. [PubMed: 18072519]

[9]. Baker ME, et al. Contrast-to-noise ratio and low-contrast object resolution on full- and low-dose MDCT: SAFIRE versus filtered back projection in a low-contrast object phantom and in the liver. AJR Am J Roentgenol. 2012; 199(1):8–18. [PubMed: 22733888]

[10]. Goenka AH, et al. Effect of reduced radiation exposure and iterative reconstruction on detection of low-contrast low-attenuation lesions in an anthropomorphic liver phantom: an 18-reader study. Radiology. 2014; 272(1):154–63. [PubMed: 24620913]

[11]. Schindera ST, et al. Iterative reconstruction algorithm for CT: can radiation dose be decreased while low-contrast detectability is preserved? Radiology. 2013; 269(2):511–8. [PubMed: 23788715]

[12]. Boedeker KL, McNitt-Gray MF. Application of the noise power spectrum in modern diagnostic MDCT: Part II. Noise power spectra and signal to noise. Phys Med Biol. 2007; 52(14):4047–61. [PubMed: 17664594]

[13]. Wunderlich A, Noo F. Image covariance and lesion detectability in direct fan-beam x-ray computed tomography. Phys Med Biol. 2008; 53(10):2471–93. [PubMed: 18424878]

[14]. Richard S, Siewerdsen JH. Comparison of model and human observer performance for detection and discrimination tasks using dual-energy x-ray images. Med Phys. 2008; 35(11):5043–53. [PubMed: 19070238]

[15]. Yu L, et al. Prediction of human observer performance in a 2-alternative forced choice low-contrast detection task using channelized Hotelling observer: Impact of radiation dose and reconstruction algorithms. Med Phys. 2013; 40(4):041908. [PubMed: 23556902]

[16]. Leng S, et al. Correlation between model observer and human observer performance in CT imaging when lesion location is uncertain. Medical Physics. 2013; 40(8):081908. [PubMed: 23927322]

[17]. Zhang Y, et al. Correlation between human and model observer performance for discrimination task in CT. Physics in Medicine and Biology. 2014; 59(13):3389–404. [PubMed: 24875060]

[18]. Chen B, et al. Evaluating iterative reconstruction performance in computed tomography. Medical Physics. 2014; 41(12):121913. [PubMed: 25471973]

[19]. Solomon J, Samei E. Quantum noise properties of CT images with anatomical textured backgrounds across reconstruction algorithms: FBP and SAFIRE. Medical Physics. 2014; 41(9): 091908. [PubMed: 25186395]

[20]. Matsumoto J, et al. Three-Dimensional Physical Modeling: A Primer for Radiologists. Radiographics. 2015 In Press.

[21]. Miller MA, Hutchins GD. Development of anatomically realistic PET and PET/CT phantoms with rapid prototyping technology. Nuclear Science Symposium Conference Record, 2007. NSS'07. IEEE. 2007; 6:4252–4257.

[22]. Yoo TS, et al. Toward quantitative X-ray CT phantoms of metastatic tumors using rapid prototyping technology. Biomedical Imaging: From Nano to Macro, 2011 IEEE International Symposium on. 2011:1770–1773.

[23]. Solomon J, Bochud F, Samei E. Design of anthropomorphic textured phantoms for CT performance evaluation. SPIE Medical Imaging. 2014 90331U-90331U-11.

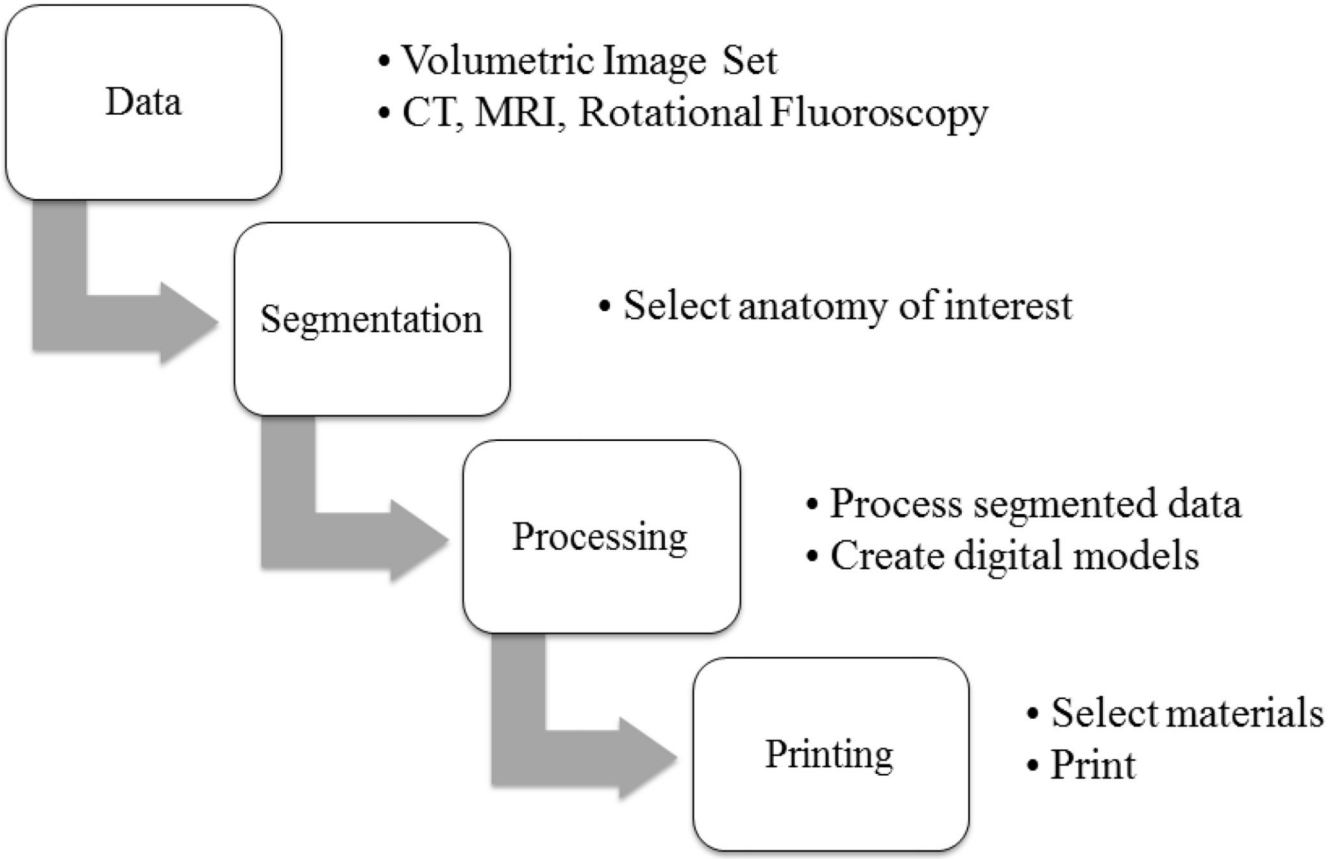

Figure 1.
A flow chart of general procedure of 3D printing.

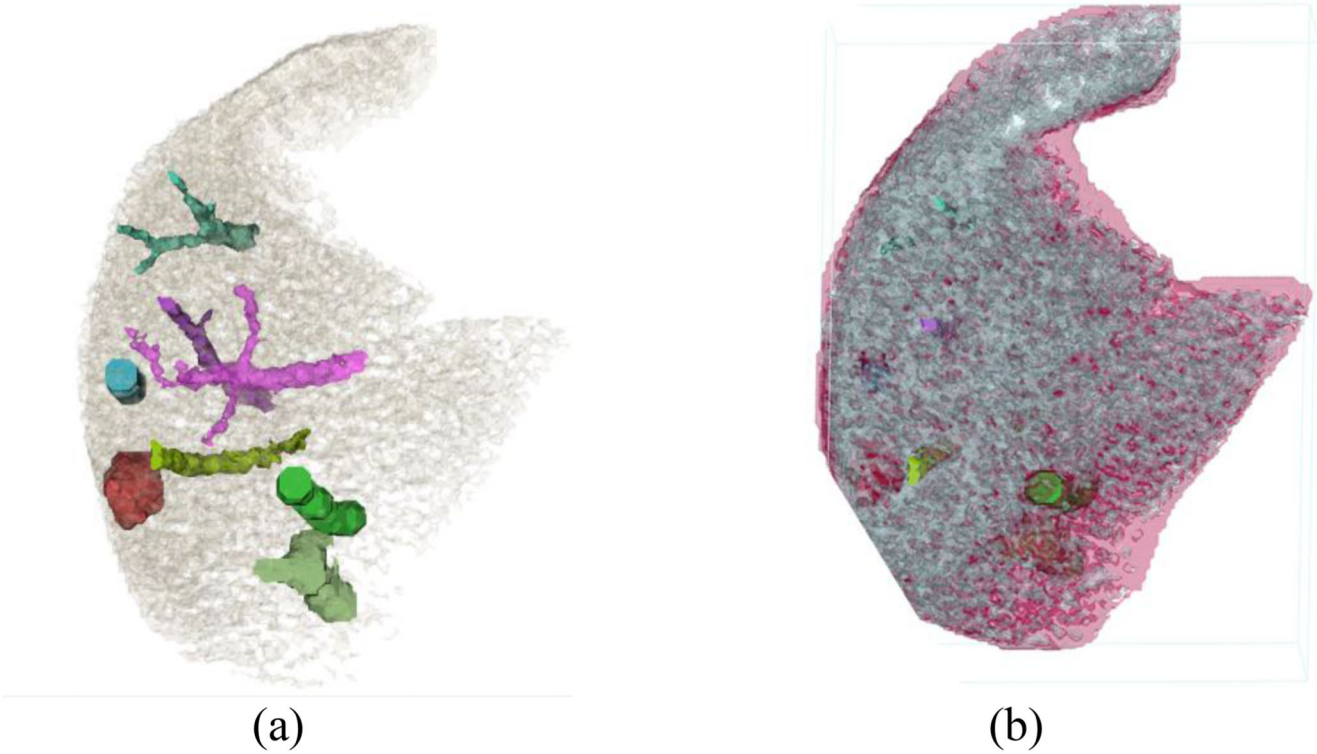

Figure 2.
Digital models were created for each segmented vessels and lesions (a). Liver tissues were assigned to 2 materials to simulate heterogeneous background (b).

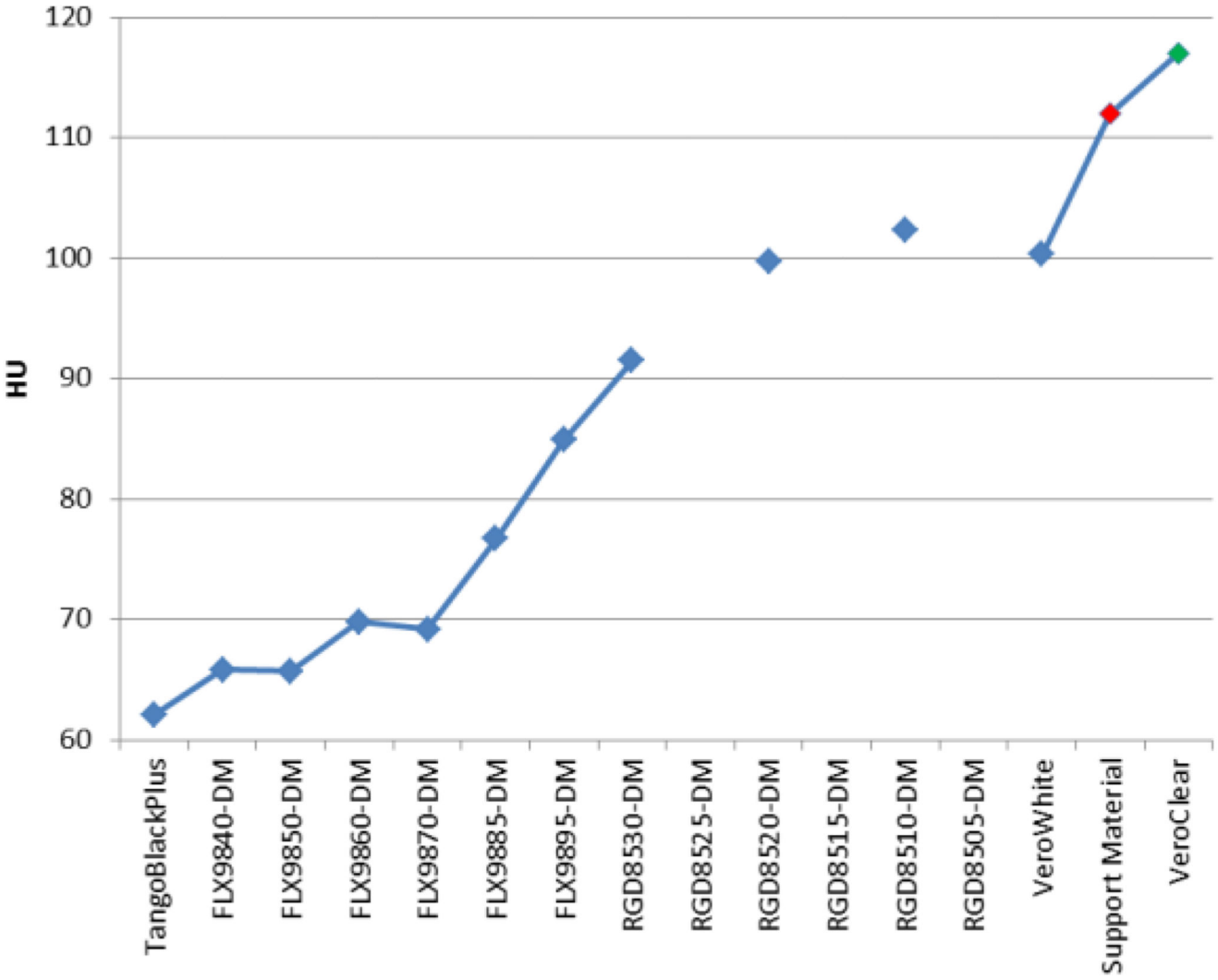

Figure 3.
CT numbers of available printing materials.

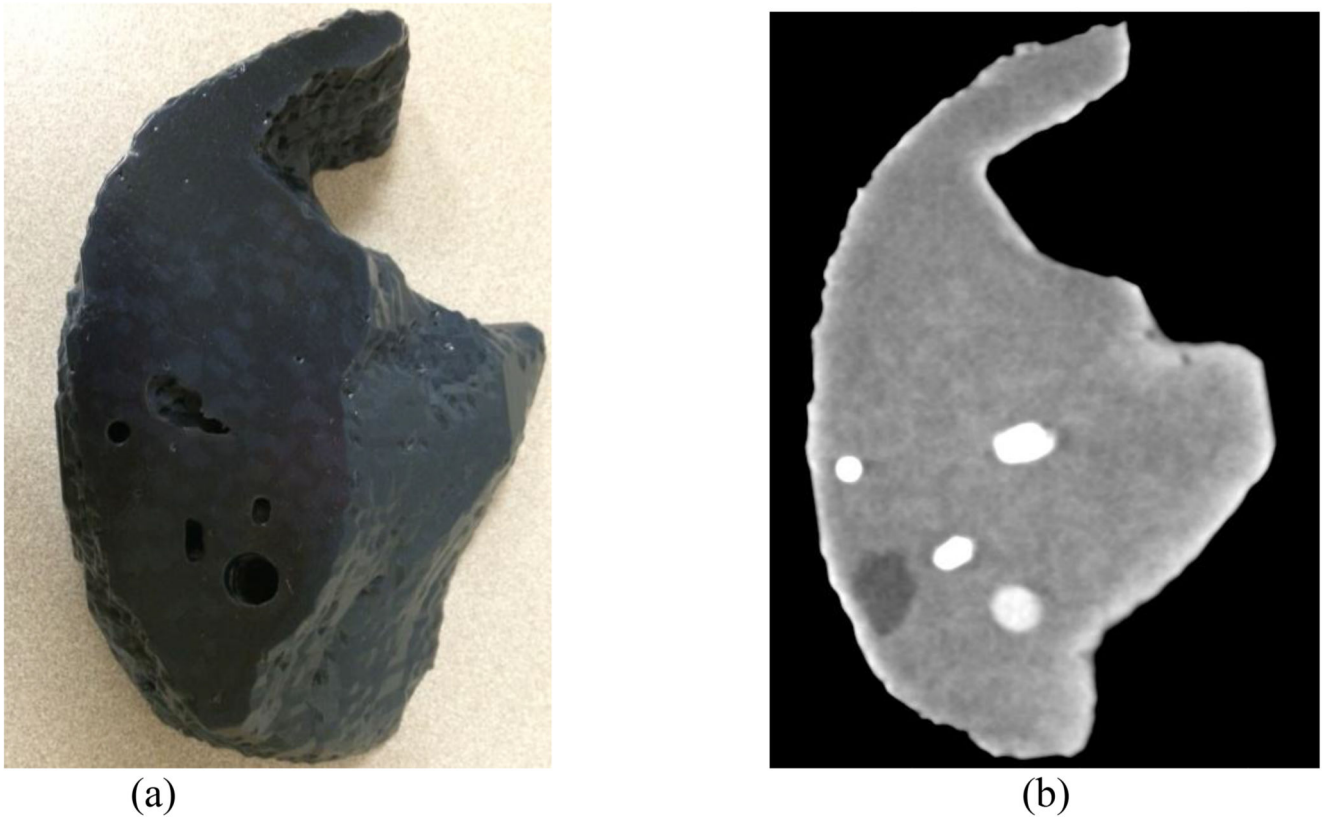

Figure 4.
Photograph (a) and CT image (b) of the printed liver phantom. The display window width and window center are 100HU and 80HU.

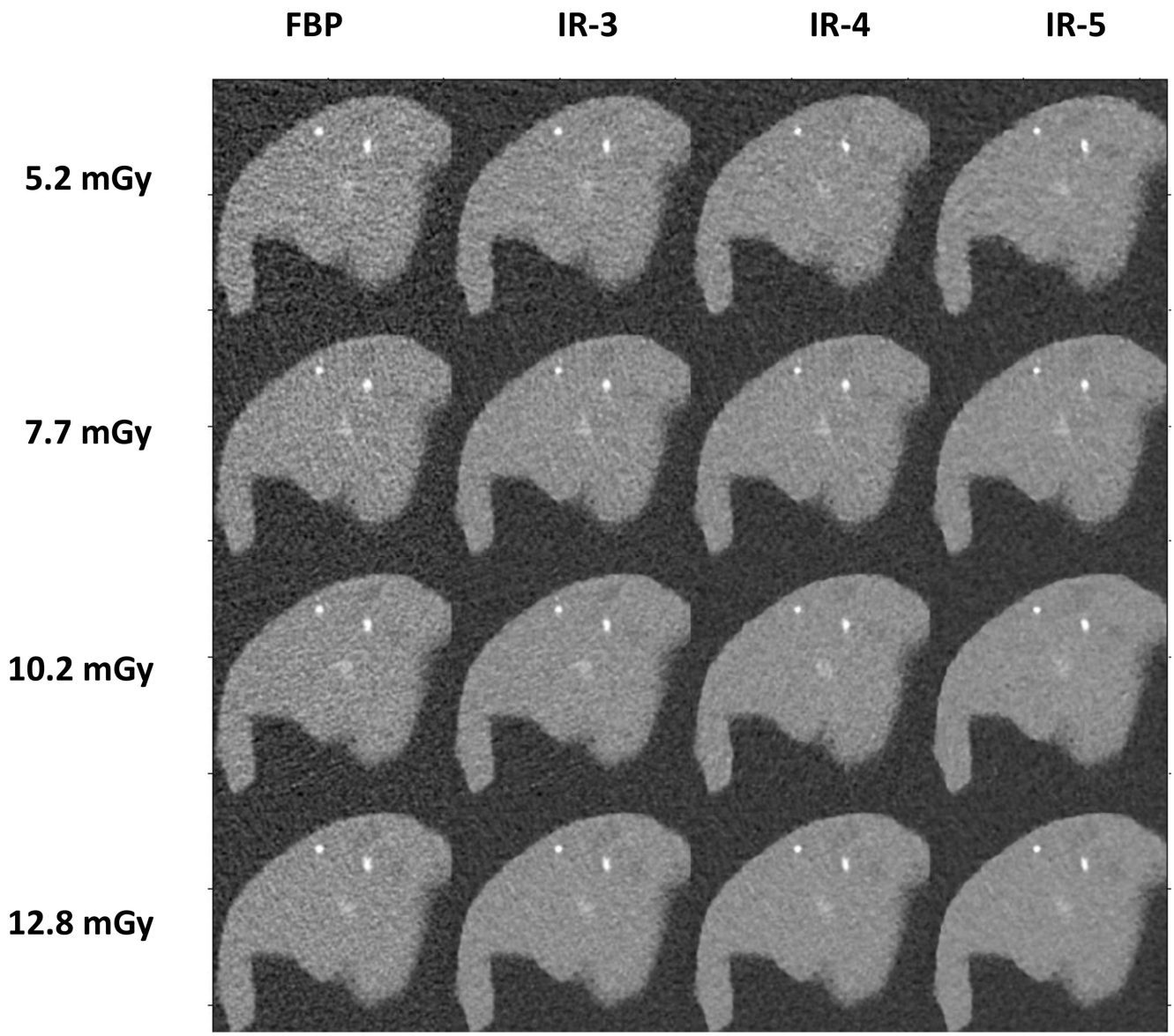

Figure 5.
CT images of the liver phantom scanned at 4 dose levels and reconstructed with 4 reconstruction algorithms.

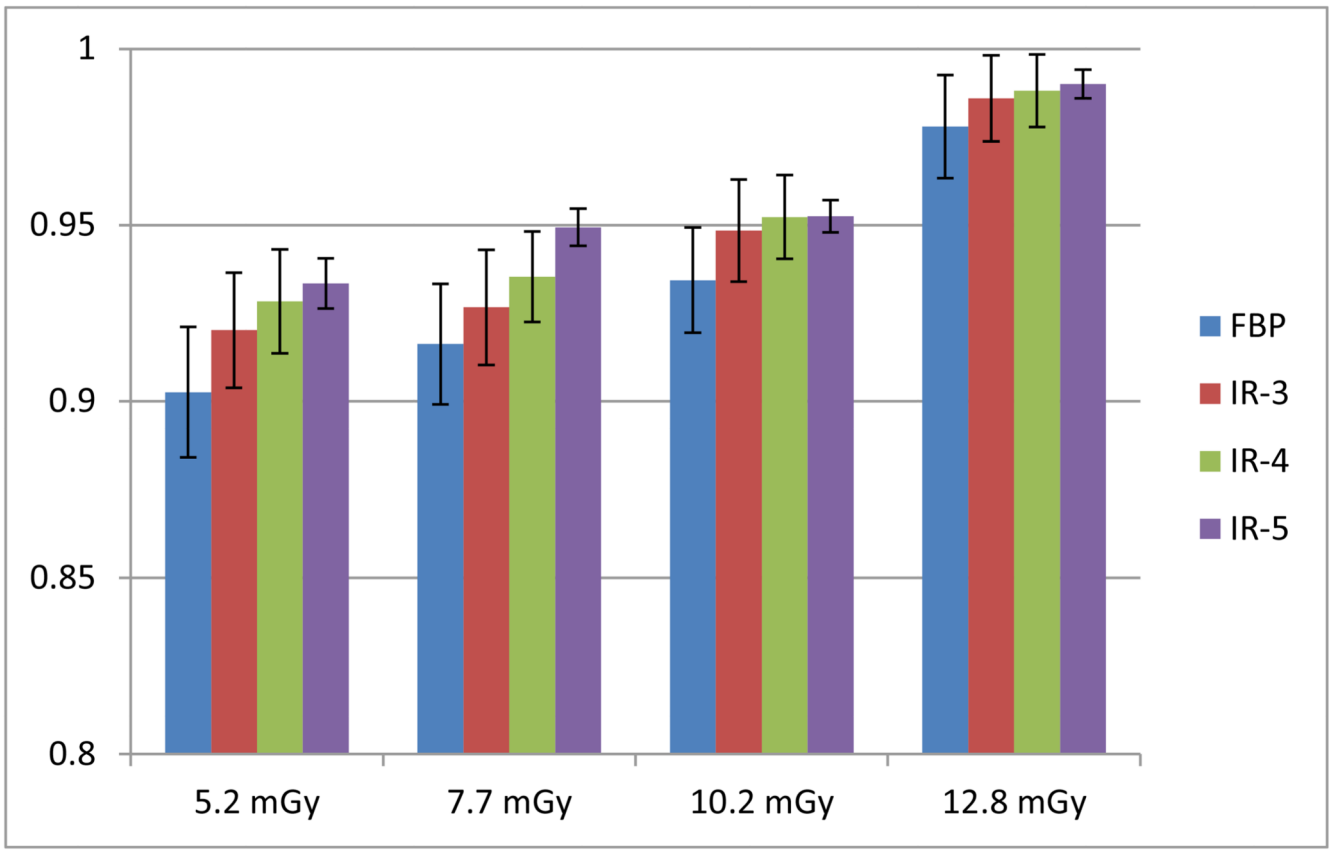

Figure 6.
AUC values of CHO on images obtained at 4 dose levels and 4 reconstruction algorithms.